

Eurasian Journal of Physics and Functional Materials

2021, 5(1), 6-14

Non-destructive analysis of materials by neutron imaging at the TITAN facility

K.M. Nazarov^{*,1,2,3}, B. Mukhametuly^{1,3,4}, S.E. Kichanov²,
T.K. Zholdybayev^{1,4}, A.A. Shaimerdenov¹, K.B. Karakozov¹,
D.S. Dyussambayev¹, M.T. Aitkulov¹, M. Yerdauletov^{1,2,3},
P. Napolskiy⁵, M. Kenessarlin^{2,5}, E.K. Kalymkhan⁴,
N.A. Imamverdiyev⁶, S.H. Jabarov⁷

¹Institute of Nuclear Physics, Almaty, Kazakhstan

²Joint Institute for Nuclear Research, Dubna, Russia

³L.N. Gumilyov Eurasian National University, Nur-Sultan, Kazakhstan

⁴Al-Farabi Kazakh National University, Almaty, Kazakhstan

⁵Dubna State University, Dubna, Russia

⁶Baku State University, Baku, Azerbaijan

⁷Azerbaijan State Pedagogical University, Baku, Azerbaijan

e-mail: knazarov@jinr.ru

DOI: 10.32523/ejpfm.2021050101

Received: 25.01.2021 - after revision

Since 2019, the TITAN neutron radiography and tomography facility have been operating at the WWR-K research reactor. The experimental station is intended for a wide range of applications in various fields of science. Since the launch, several interesting works have been carried out to study the internal features of lithium-ion batteries and geophysical materials. The spatial resolution of the detector system was sufficient to visualize the internal elements of the lithium battery and to separate individual grains of the pyrite mineral in the rock sample. This paper presents the technical parameters of the experimental setup and the results of the recent applied research.

Keywords: thermal neutrons, imaging, radiography, tomography, lithium-ion battery, pyrite-rich rock.

Introduction

Neutron radiography – is one of the promising developing methods of non-destructive testing to study the inner structural features of the materials [1]. This method consists in obtaining neutron images of the studied objects. The difference in neutron macroscopic cross sections for different elements provides information on the internal distribution of inhomogeneities in the studied materials [2]. The special case of the neutron radiography method is neutron computed tomography, in which a three-dimensional model of the object is reconstructed from a set of separate radiographic images obtained at different angular positions of the sample relative to the direction of the neutron beam [3].

At the Institute of Nuclear Physics (INP) of the Ministry of Energy of the Republic of Kazakhstan (Almaty), one of the basic facilities is the steady-state research nuclear reactor WWR-K, which carries out fundamental nuclear physical and material research, testing of structural and functional materials for fission and fusion reactors as well as produces radioisotopes for medicine and industry [4-6]. As early as 1978, the first AGAVA neutron imaging instrument was mounted on the 2-nd neutron beam port of the WWR-K reactor. The AGAVA was developed for the study of irradiated nuclear fuel and components. Foil-film transfer technique was used for imaging of examination fuel. Nowadays, this instrument is already obsolescence and requires updating the main components; therefore, it is under an extended shutdown.

Wide application capability and relevance for scientific research of neutron radiography and tomography methods have become the main motivation for the build-up of a new instrument at the Institute of Nuclear Physics, Almaty [7-14]. In 2019, a new experimental station TITAN (Transmission Imaging with Thermal Neutrons) was put into operation at the research reactor WWR-K, to conduct research on non-destructive testing of materials using neutron radiography and tomography [15-16]. The neutron radiography and tomography instrument are located in horizontal channel No. 1 of the WWR-K research reactor.

In this paper, we describe in detail the design of the TITAN facility and the results of recent applied research.

Characteristics of the TITAN facility

The layout TITAN facility is shown in Figure 1. The neutron spectrum of the facility is mainly determined by the type of reactor, in our case, WWR-K is a reactor with thermal neutrons because the reactor uses light water as a moderator [17-18]. The spectra of neutron and gamma radiation simulated using the MCNP (Monte-Carlo N-Particle transport code) program for channel No. 1 of the WWR-K reactor is shown in Figure 2. Since the instrumentation is located on a radial beam port that directly views the core, the neutron beam contains a significant portion of the unwanted background of fast neutrons and gamma rays. There are several solutions for this case: a neutron guide or neutron filters. Due to the limited space in the experimental hall of the WWR-K reactor, we decided

to use neutron filters. The use of a beam filter gives us the opportunity to: reduce the background near the detector system and reduce the thickness of biological shielding, protect workers/staff from radiation. In references [19-21], various possible options for fast neutron filters, including silicon, quartz, sapphire, bismuth, and lead were considered. Single-crystal sapphire with a thickness of 105 mm was selected as a fast neutron filter due to its proven quality as a filter at room temperature, unlike other materials [22-24]. Therefore, after the beam shutter, a single-crystal sapphire filter with a thickness of 105 mm has been installed.

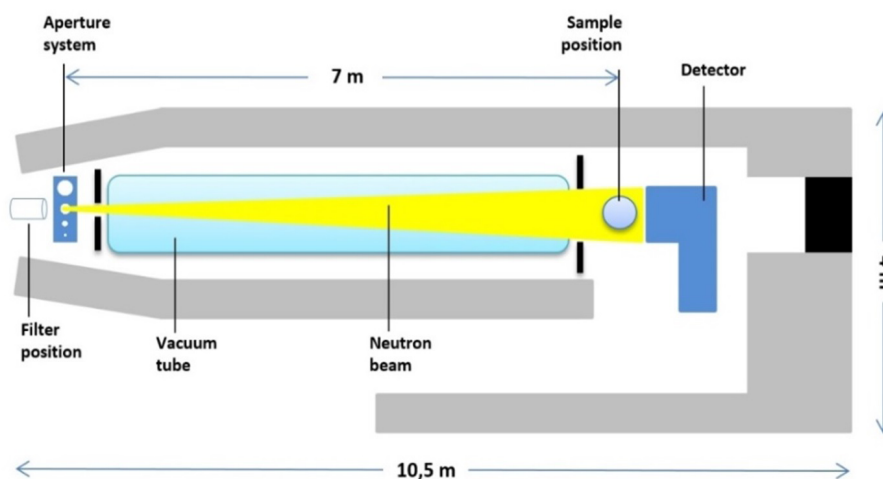


Figure 1. The layout of TITAN neutron imaging facility at the WWR-K reactor.

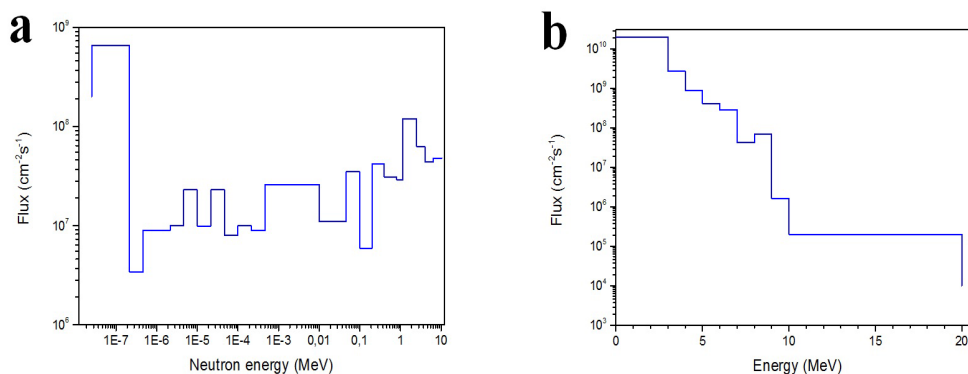


Figure 2. The spectra of (a) neutron and (b) gamma radiation simulated using the MCNP program for channel No. 1 of the WWR-K reactor.

At this facility, a neutron beam with dimensions up to $200 \times 200 \text{ mm}^2$ is formed by a collimator system and an evacuated tube to reduce the intensity loss due to neutron scattering in the air. The characteristic parameter L/D is determined by the ratio of the distance L between the entrance aperture of the collimator system and the sample position to the diameter of the entrance aperture of the collimator D . The corresponding values for the created setup are $L=7 \text{ m}$, $D=2 \text{ cm}$, which corresponds to the value of the parameter $L/D=350$. This value is at the level of similar installations in other world neutron centers [25,

26]. Additionally, a system for varying the diameter D of the entrance aperture of the collimator system from 5 to 90 mm was installed, which will allow operation in a wide range of the characteristic L/D parameter from 75 to 1400. A special detector based on a two-mirror optical scheme is used to obtain neutron radiographic images. The neutron beam passing through the studied object is transformed into a light signal using a scintillation screen, which is focused by the lens onto the CCD-matrix of a high-sensitivity video-camera. The lens with a variable focal length of 70-300 mm (TAMRON AF) is installed in front of the camera, as a result of which the field of view of the detector can be varied from 50×50 to 200×200 mm² with a resulting pixel size from 25×25 to 97×97 μm^2 . The tomographic measurements at the experimental facility are carried out using a goniometer system with a rotating table of the KOHZU Company from Japan. Minimum step of rotation 0.002 degrees.

Table 1. The main parameters of the neutron imaging facility TITAN.

Spectrum	Thermal neutrons
Distance moderator-pinhole	3.5 m
Distance pinhole-sample L	7 m
Aperture diameter D	5, 10, 20, 40, 90 mm
L/D ratio	1400, 700, 350, 175, 75
Field-of-view	from 50×50 to 200×200 mm ²
Scintillation screens	⁶ LiF/ZnS:Ag and Gadox
CCD-chip of camera	HAMAMATSU-chip, 2k*2k pixels, Full size 24×24 mm ²
Lens system	70-300 mm with variable focal length
Pixel size	25-100 μm
Neutron flux	1.1×10^8 n/(cm ² *sec.) at $L/D=100$ 1.2×10^7 n/(cm ² *sec.) at $L/D=350$
Typical exposure time	1-30 sec.

In the works presented below, tomographic experiments were carried out with a rotation step of 0.5° , and the total number of measured angular projections was 360. The exposure time for one projection was 20 sec., and the resulting measurements lasted 4 hours. Radiographic angular projections were corrected by subtracting the camera dark current image and normalized to the incident neutron beam using ImageJ software [27]. Tomographic reconstruction was performed using the STP software [28]. The Oimoen algorithm was used to reduce ring artifacts [29]. The size of one voxel in our research is $45 \times 45 \times 45$ microns. 3D voxel volume data describe the spatial distribution of neutron attenuation coefficient values within the entire volume. FEI AVISO 3D 8.1 software was used to visualize and analyze the reconstructed 3D data.

Application example

Neutron radiography and tomography as one of the non-destructive testing methods for assessing the quality of a product and parts are important in many areas of industry. It is also a complementary technique for the well-known X-ray radiography. Due to the difference in the nature of the interaction of neutron and X-ray radiation with the substance of the sample under study, it gives a different contrast in the obtained experimental images. In these methods, the resulting transmitted image is directly related to the characteristics of an object in real scale. In particular, neutron radiography has attracted attention as a useful test method, since neutrons have deep-penetrating power, different cross-sections for the interaction of a neutron with elements, as well as isotopes of one element, sensitivity to light elements such as hydrogen, boron, and lithium. This means that the method can non-destructively evaluate the microstructural characteristics of the sample and the distribution of the material in it, which makes this method attractive for the analysis of industrial products [30-33].

Li-ion battery

One of the promising and priority areas of application of neutron methods of non-destructive testing is the study of the microstructure of chemical current sources, in particular, lithium-ion batteries. Recently, neutron radiography and tomography have found wide application in research of the dynamic process of Li diffusion and expansion of electrodes [34-36], electrolyte consumption [37] and gas evolution [38-39].

In this study, we chose a lithium-ion battery (LIB) of coin-cell type as a test sample. The specific characteristics of the batteries are determined, first of all, by the specific characteristics of the electrode materials. The main direction of research aimed at improving the specific energy storage of lithium-ion batteries is associated with the search for new cathode and anode materials capable of providing higher specific capacities and a large potential difference [40-41].

The electrode preparation procedure included several stages. At the first stage, the cathode paste was prepared, consisting of LTO –lithium titanate oxide powder, a conductive additive, and a polymer binder. Carbon nanotubes, carbon black TimcalSuperC45, were used as conductive additives. Polyvinylidene fluoride, hsv-900 (Kynar) was used as a polymer binder. The dry components were added N – methyl pyrrolidone, and then the solution was subjected to mechanical stirring for 12 hours at a temperature of 60 C. In this case, the mass loading of each of their dry components was determined by the ratio of 88.5Coin cells 2032 were galvanostatically tested on an 8-channel analyzer of MTI-BST8-MA power supplies in the voltage range of 2-4 V. The cell charge/discharge current was set at 10 mA per gram of the cathode coating.

The neutron tomography method was used to visualize the lithium distribution regions flowing inside the cell in the initial and final states of lithium-ion batteries. Figure 3 shows a photograph of a lithium-ion battery, radiographic images and a slice of a 3D model at the initial stage, and after 50 charge-recharge

cycles.

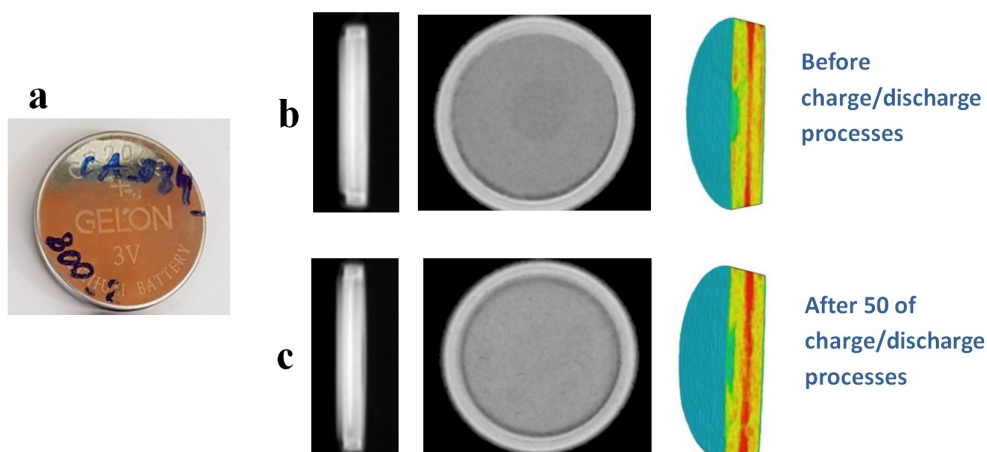


Figure 3. a) The photograph of a lithium-ion battery, b) radiographic images and a slice of a 3D model at the initial stage, and c) radiographic images and a slice of a 3D model after 50 charge-recharge cycles.

Figure 3-b shows a three-dimensional model of the battery, the main internal elements are clearly visible and distinguishable due to the strong attenuation of a neutron by lithium atoms: anode (metallic lithium) and cathode layers (LTO), steel gasket. The aluminium body is practically invisible due to the weak attenuation of the neutron. Figure 3-c shows a slice of a 3D model of a lithium-ion cell obtained after 50 charge/discharge cycles. The LTO cathode material located in the middle has good contrast. An increase in the thickness and attenuation coefficient of the neutron by the cathode material is observed. When analyzing the three-dimensional model, the change in the volume of the cathode layers was calculated in connection with the distribution of lithium and electrolyte over the volume of batteries, in the initial state and after 50 charge-recharge cycles, in which the volume increased 2.6 times. Consequently, the thickness of these cathode layers changed and increased 1.52 times in relation to the initial state.

Geological object

In this work, we demonstrate the use of neutron radiography and tomography methods for the structural characterization of rock materials. Using these methods, the internal structure of pyrite-rich rock was studied. Due to the highly penetrating ability of neutrons, it is possible to obtain a neutron image of the investigated materials of a rather large size [42]. Based on the difference in the thermal neutron attenuation coefficient of rock constituents and the use of modern mathematical algorithms for the analysis of three-dimensional (3-D) image data, it was possible to obtain the spatial distribution of pyrite in studied rock sample taken from place of ejections of mud volcanoes in Azerbaijan. Also, volumetric measurements were carried out, namely, distributions of volumes, average sizes parameters grains of pyrite were obtained.

A photograph, a neutron radiographic image and slices of the reconstructed three-dimensional model of a pyrite-rich rock are shown in Figure 4. Bright areas correspond to high attenuation of neutrons in pyrite grains. Dark areas are region

with low neutron attenuation. The background is black. The three-dimensional

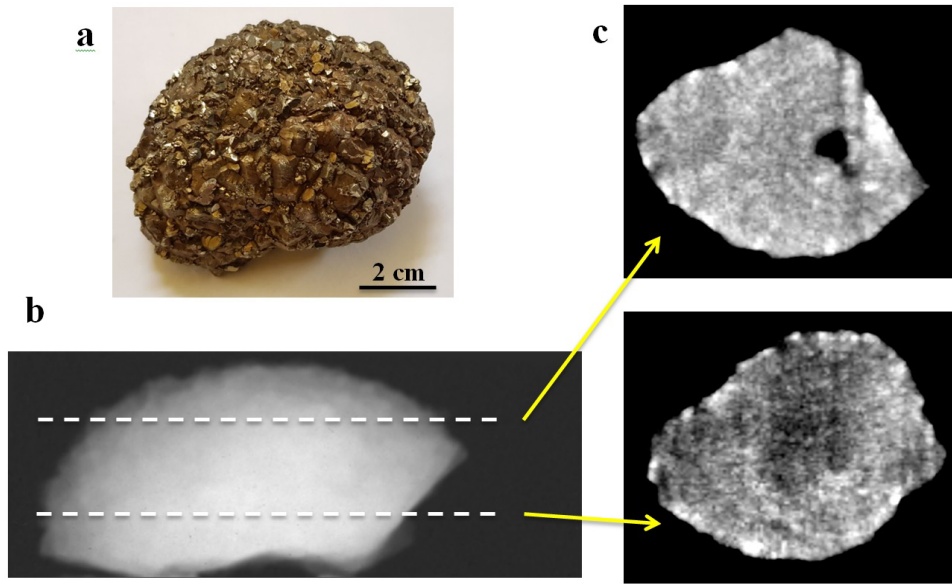


Figure 4. a) The photograph, b) neutron-radiographic image and c) a slice of a 3D model pyrite bulk rock. The slices correspond to the bottom and upper parts of the studied rock fragment.

model of the rock reconstructed from the neutron tomography data is shown in Figure 5-a. the process of segmentation by the attenuation coefficient helped to separate the grains of pyrite mineral from the total volume of the sample. Pyrite grains are well discernible (Figure 5 b-c). Figure 5-c shows a three-dimensional model of a pyrite grain sample after the separation process. To improve the perception of the spatial distribution of grains, they are painted in different colours depending on the volume of the grains. These grains are crystals of various shapes. The distribution of grains by volume is shown on the Figure 5-d and the grain volumes are concentrated in the range from 0.12 to 6 mm^3 . Several larger clusters ranging in size from 10 to 25 mm^3 were also observed. The distributions of the equivalent radius were calculated, this is the radius of the sphere with the equivalent volume of the observed grains. The equivalent diameter or average grain size of pyrite minerals ranges from 0.6 to 1.5 mm (Figure 5-e).

Conclusion

This article describes the recently developed TITAN neutron imaging facility at the WWR-K reactor. The design of the facility, a detailed description of the main components and technical parameters are presented. Today, the TITAN neutron imaging facility operates for scientific use. During the first two years of operation, several interesting studies were carried out on various topics. In this work, it was possible to three-dimensionally reconstruct the internal elements of a lithium-ion battery and to visualize changes in the thickness of cathode materials during charging/recharging process, as well as to study the spatial distribution of grains of pyrite minerals in the rock and calculate its volumetric parameters.

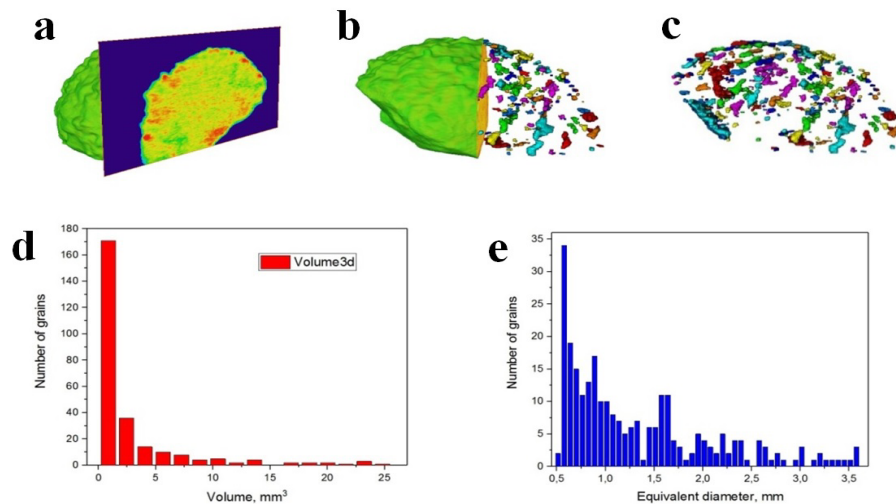


Figure 5. a) An example of a slice cut of the three dimensional model; b-c) 3D model of separated grains of pyrite mineral after segmentation processes. Colours correspond to different grain sizes; d-e) Distribution of grains of the pyrite by volume and equivalent diameter.

These studies are very useful for increasing the potential and expanding the applications of the TITAN neutron imaging facility.

Acknowledgments

This work was supported by a grant from the Plenipotentiary Representative of the Republic of Kazakhstan at the JINR, Russia (No. 391 from 20.07.2020, paragraph 8).

References

- [1] P. Vontobel et al., *Physica B Condens. Matter* **385-386** (2006) 475-480.
- [2] K.M. Podurets et al., *Crystallography Reports* **66(2)** (2021) 256-270.
- [3] N. Kardjilov et al., *Mater. Today* **14** (2011) 248-256.
- [4] A. Shaimerdenov et al., *Fusion Sci. Technol.* **76(3)** (2020) 304-313.
- [5] A.S. Larionov et al., *Mater. Sci. Forum* **945** (2018) 660-664.
- [6] M.S. Merezhko et al., *Phys. Met. Metallogr.* **120** (2019) 716-721.
- [7] T.I. Ivankina et al., *Nature Sci. Rep.* **10** (2020) 12869.
- [8] A. El Abd et al., *Appl. Radiat. Isot.* **156** (2020) 105970.
- [9] S.E. Kichanov et al., *Rom. J. Phys.* **64** (2019) 803.
- [10] K.M. Nazarov et al., *Eurasian Phys. Tech. J.* **17(1)** (2020) 39-45.
- [11] A. El Abd et al., *Constr. Build. Mater.* **256** (2020) 119471.
- [12] S.E. Kichanov et al., *J. Imaging* **4(2)** (2018) 25.
- [13] G. Abramson et al., *J. Surf. Invest.: X-ray Synchrotron Neutron Tech.* **12** (2018) 114-117.
- [14] S.E. Kichanov et al., *Physics of Particles and Nuclei Letters* **17(1)** (2020) 73-78.
- [15] K.M. Nazarov, *Nucl. Instrum. Methods. Phys. Res. A* **982** (2020) 164572.

- [16] B. Muhametuly et al., *J. Surf. Invest.: X-ray, Synchrotron Neutron Tech.* **13**(5), (2019) 877-879.
- [17] A.A. Shaimerdenov et al., *Phys. At. Nucl.* **81** (2018) 1-4.
- [18] A.A. Shaimerdenov et al., *At. Energy* **123** (2017) 15-20.
- [19] H.F. Nieman et al., *Rev. Sci. Instrum.* **51** (1980) 1299-1303.
- [20] J.P. Barton, *Non-destruct. Test. Evaluation* **16** (2001) 95-110.
- [21] O. Aizawa et al., *J. Nucl. Sci. Tech.* **23** (1986) 562-564.
- [22] R. Born et al., *Nucl. Instrum. Methods. Phys. Res. A* **262** (1987) 359-365.
- [23] M. Adib et al., *Czech. J. Phys.* **55** (2005) 563-578.
- [24] D. F. R. Mildner et al., *J. Appl. Cryst.* **31** (1998) 835-840.
- [25] E.H. Lehmann et al., *Neutron News* **26** (2015) 6-10.
- [26] E.H. Lehmann et al., *J. Imaging* **4-2** (2018) 52.
- [27] C. A. Schneider et al., *Nat. Methods* **9** (2012) 671-675.
- [28] F. Brun et al., *Adv. Struct. Chem. Imaging* **3**(4) (2017) 1-9.
- [29] M.J. Oimoen, *Proceedings of the Fourteenth International Conference on Applied Geologic Remote Sensing, Las Vegas, Nevada* (2000) 311-319.
- [30] K.M. Nazarov et al., *Eurasian J. Phys. Funct. Mater.* **4**(2) (2020) 122-131.
- [31] U. Garbe et al., *Phys. Procedia* **88** (2017) 13-18.
- [32] C. Grunzweig et al., *Phys. Procedia* **43** (2013) 231-242.
- [33] E.H. Lehmann et al., *EPJ Web Conf.* **104** (2015) 01007.
- [34] J.B. Siegel et al., *J. Electrochem. Soc.* **158** (2011) A523-A528.
- [35] J.B. Siegel et al., *J. Electrochem. Soc.* **160** (2013) A1031-A1038.
- [36] H. Zhou et al., *ACS Energy Lett.* **1** (2016) 981-986.
- [37] M. Lanz et al., *J. Power Sources* **101** (2001) 177-181.
- [38] B. Michalak et al., *Anal. Chem.* **88** (2016) 2877-2883.
- [39] D. Goers et al., *J. Power Sources* **130** (2004) 221-226.
- [40] F. Napolskiy et al., *Energy Technol.* **8**(6) (2020) 2000146.
- [41] M.V. Avdeev et al., *J. Surf. Invest.: X-ray, Synchrotron Neutron Tech.* **13**(4) (2019) 614-618.
- [42] I.Y. Zel et al., *Acta Geodyn. Geomater.* **17**(3) (2020) 259-267.